Available online at www.sciencedirect.com
SCIENCE DIRECT®
Journal of Sound and Vibration 277 (2004) 691–710
JOURNAL OF SOUND AND VIBRATION
www.elsevier.com/locate/jsvi

Micro-control actions of actuator patches laminated on hemispherical shells

P. Smithmaitrie, H.S. Tzou*

StrucTronics Lab, Department of Mechanical Engineering, University of Kentucky, Lexington, KY 40506-0503, USA

Received 20 May 2002; accepted 5 September 2003

Abstract

Spherical shell-type structures and components appear in many engineering systems, such as radar domes, pressure vessels, storage tanks, etc. This study is to evaluate the micro-control actions and distributed control effectiveness of segmented actuator patches laminated on hemispheric shells. Mathematical models and governing equations of the hemispheric shells laminated with distributed actuator patches are presented first, followed by formulations of distributed control forces and micro-control actions including meridional/circumferential membrane and bending control components. Due to difficulties in analytical solution procedures, assumed mode shape functions based on the bending approximation theory are used in the modal control force expressions and analyses. Spatially distributed electromechanical actuation characteristics resulting from various meridional and circumferential actions of segmented actuator patches are evaluated. Distributed control forces, patch sizes, actuator locations, micro-control actions, and normalized control authorities of a free-floating hemispheric shell are analyzed in case studies. Parametric analysis indicates that (1) the control forces and membrane/bending components are mode and location dependent, (2) actuators placed near the free boundary contributes the most significant control actions, and (3) the meridional/circumferential membrane control actions dominate the overall control effect.

1. Introduction

Radar domes, pressure vessels, storage tanks, etc. often take the form of spherical shells. Dynamic characteristics and vibrations of spherical shells and structures have been investigated over the years [1–5]. Natural frequencies of a shallow spherical shell and a thin hemisphere shell with free boundary condition have been investigated and experimentally verified [6,7]. Dynamic

*Corresponding author. Tel.: +1-606-257-6336; fax: +1-606-257-3304.
E-mail address: hstzou@engr.uky.edu (H.S. Tzou).

0022-460X/$ - see front matter © 2003 Elsevier Ltd. All rights reserved.
doi:10.1016/j.jsv.2003.09.016

modal sensing characteristics, distributed modal voltages, and micro-signal components of spherical shells of revolution laminated with distributed piezoelectric sensor layers were recently investigated [8]. Actuations of spherical shells with piezoceramic actuators were also studied [9–11], so the conical shells and deep paraboloidal shells [12,13]. This study evaluates microscopic electromechanical actuation and control effectiveness of segmented patch actuators laminated on hemispherical shells.

Mathematical modelling of spherical shells coupled with distributed actuators is presented first, followed by the analysis of actuator induced forces and micro-control actions respectively in the meridional, circumferential, and transverse directions. In order to evaluate modal dependent distributed micro-control actions, assumed mode shape functions based on the bending approximation theory are used in the formulation of control forces and their contributing microscopic actions in the modal domain. Detailed control forces, contributing meridional and circumferential membrane/bending micro-control actions, and normalized control effects of free-hemispheric shells with various design parameters (e.g., actuator patch locations, shell thickness, and shell radius of curvature, etc.) are evaluated in case studies.

2. Segmented distributed actuator patches on spherical shell

It is assumed that an arbitrary segmented piezoelectric actuator patch defined from ϕ_1 to ϕ_2 in the meridional direction and from ψ_1 to ψ_2 in the circumferential direction is laminated on the hemispherical shell; Fig. 1. By the thin shell approximation, the radius of curvature of the actuator patch is $(R + h/2 + h^a/2) \approx R$, and the effective actuator area is approximately $R^2(\psi_2 - \psi_1)(\cos\phi_1 - \cos\phi_2)$.

If the electrode resistance is neglected, the control voltage on the segmented patch is constant. Thus, an actuator control voltage $\phi^a(\phi, \psi, t)$ applied to the distributed actuator patch can be defined by

$$\phi^a(\phi, \psi, t) = \phi^a(t)[u_s(\phi - \phi_1) - u_s(\phi - \phi_2)][u_s(\psi - \psi_1) - u_s(\psi - \psi_2)], \tag{1}$$

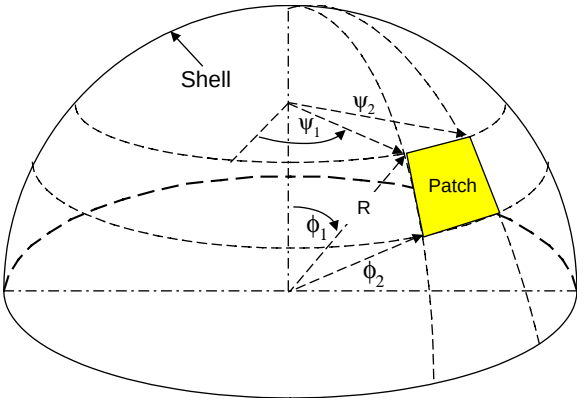

Fig. 1. An arbitrary actuator patch laminated on a hemispheric shell.

where the superscript "a" denotes the induced actuator voltage; $u_s(\cdot)$ is a unit step function, $u_s(\phi - \phi^*) = 1$ when $\phi \geqslant \phi^*$, and $= 0$ when $\phi < \phi^*$. Accordingly, control actions induced by the actuator patch include a control force $N^c_{\phi\phi}$ in the ϕ-direction, a control force $N^c_{\psi\psi}$ in the ψ-direction, a control moment $M^c_{\phi\phi}$ in the ϕ-direction, and a control moment $M^c_{\psi\psi}$ in the ψ-direction respectively and they are defined by

$$N^c_{\phi\phi} = Y_p d_{31}\phi^a[u_s(\phi-\phi_1) - u_s(\phi-\phi_2)][u_s(\psi-\psi_1) - u_s(\psi-\psi_2)], \tag{2}$$

$$N^c_{\psi\psi} = Y_p d_{32}\phi^a[u_s(\phi-\phi_1) - u_s(\phi-\phi_2)][u_s(\psi-\psi_1) - u_s(\psi-\psi_2)], \tag{3}$$

$$M^c_{\phi\phi} = r^a_1 Y_p d_{31}\phi^a[u_s(\phi-\phi_1) - u_s(\phi-\phi_2)][u_s(\psi-\psi_1) - u_s(\psi-\psi_2)], \tag{4}$$

$$M^c_{\psi\psi} = r^a_2 Y_p d_{32}\phi^a[u_s(\phi-\phi_1) - u_s(\phi-\phi_2)][u_s(\psi-\psi_1) - u_s(\psi-\psi_2)], \tag{5}$$

where Y_p is the actuator elastic modulus; d_{3i} is the piezoelectric strain constant; r^a_i defines the distance measured from the neutral surface to the mid-plane of the actuator patch (i.e., the moment arm); ϕ^a is the imposed control voltage determined by control algorithms (e.g., open-loop or closed-loop control) [14,15]. Substituting the control forces and moments into the system equations of the spherical shell/actuator system and imposing the bending approximation theory [8], i.e., $N_{\phi\phi} = N_{\psi\psi} = N_{\phi\psi} = 0$, yields the simplified governing equations:

$$\frac{\partial}{\partial\phi}(-N^c_{\phi\phi}\sin\phi) - (-N^c_{\psi\psi})\cos\phi + Q_{\phi 3}\sin\phi + Rq_\phi\sin\phi = R\sin\phi\rho h\frac{\partial^2 u_\phi}{\partial t^2}, \tag{6}$$

$$\frac{\partial}{\partial\psi}(-N^c_{\psi\psi}) + Q_{\psi 3}\sin\phi + Rq_\psi\sin\phi = R\sin\phi\rho h\frac{\partial^2 u_\psi}{\partial t^2}, \tag{7}$$

$$\frac{\partial}{\partial\phi}(Q_{\phi 3}\sin\phi) + \frac{\partial}{\partial\psi}(Q_{\psi 3}) - (-N^c_{\phi\phi} - N^c_{\psi\psi})\sin\phi + Rq_3\sin\phi = R\sin\phi\rho h\frac{\partial^2 u_3}{\partial t^2} \tag{8}$$

and

$$Q_{\phi 3} = \frac{1}{R\sin\phi}\left[\frac{\partial}{\partial\phi}((M_{\phi\phi} - M^c_{\phi\phi})\sin\phi) + \frac{\partial}{\partial\psi}(M_{\psi\phi}) - (M_{\psi\psi} - M^c_{\psi\psi})\cos\phi\right], \tag{9}$$

$$Q_{\psi 3} = \frac{1}{R\sin\phi}\left[\frac{\partial}{\partial\phi}(M_{\phi\psi}\sin\phi) + \frac{\partial}{\partial\psi}(M_{\psi\psi} - M^c_{\psi\psi}) + M_{\psi\phi}\cos\phi\right]. \tag{10}$$

The first two equations are respectively the meridional and the circumferential dynamic/control equations; the third one is the transverse dynamic/control equation; and the last two define the transverse shear effects contributed by elastic and control moments. Distributed control components appear in all three equations and thus, open- or closed-loop distributed control of spherical shells can be achieved. These three equations are fully coupled spherical shell/actuator system equations and the membrane control effects are still preserved in the system equations, although the elastic membrane forces of the spherical shell are neglected in the bending approximation. Note that the objective of this study is to evaluate spatially distributed micro-control actions of strategically placed actuator patches at various locations, not the hemispherical shell dynamics. To focus on the micro-membrane and bending control characteristics, assumed mode shape functions and natural frequencies resulting from the bending approximation theory

are used in the parametric study of modal control forces contributed by distributed actuator segments. Although the elastic membrane effects are essential to the fully-coupled shell dynamics, they are neglected in the classical bending approximation theory.

3. Analysis of control actions in modal domain

The modal expansion assumption states that the displacement response $u_i(\phi,\psi,t)$ in the ith direction of the hemispherical shell is composed of all participating modes, i.e., $u_i(\phi,\psi,t) = \sum_{k=2}^{\infty} \eta_{ik}(t)U_{ik}(\phi,\psi)$, $i = \phi,\psi,3$. Imposing the modal expansion and the modal orthogonality and including a viscous damping, one can derive the modal equation of the hemispherical shell as

$$\ddot{\eta}_k + 2\zeta_k\omega_k\dot{\eta}_k + \omega_k^2\eta_k = F_k^m(t) + F_k^c(t) \equiv \hat{F}_k(t), \tag{11}$$

where η_k is the modal participation factor; ζ_k is the damping ratio $\zeta_k = c/(2\rho h\omega_k)$; c is the damping constant; ω_k is the kth natural frequency; ρ is the mass density of the shell; $F_k^m(t)$ is the mechanical excitation; $F_k^c(t)$ is the electrical control excitation; k denotes the circumferential wave number; and $\hat{F}_k(t)$ is the total modal force. Fig. 2 shows the open-loop control of the hemispherical shell system.

Recall that the modal electric control force F_k^c induced by the piezoelectric actuator patch includes four control actions: a control force $N_{\phi\phi}^c$ in the ϕ-direction, a control force $N_{\psi\psi}^c$ in the ψ-direction, a control moment $M_{\phi\phi}^c$ in the ϕ-direction, and a control moment $M_{\psi\psi}^c$ in the ψ-direction defined previously. Although the elastic membrane forces are neglected in the bending approximation, the membrane control forces are still preserved in the system equations, such that their spatially distributed micro-control actions can still be evaluated. The assumed mode shape functions based on the bending approximation theory are used to evaluate modal control forces and microscopic control actions. The micro-control actions of actuator patches depend on actuator characteristics, spatial locations, and modal behavior. Although the elastic membrane effect of the shell will affect the modal behavior, it does not explicitly appear in micro-control actions of actuator patches. Detailed modal control forces and micro-control actions of spherical actuator patches are analyzed next.

3.1. Modal characteristics and modal control forces

Evaluation of modal micro-sensing and actuation characteristics of distributed and segmented sensors/actuators depends on fundamental structural dynamics and free-vibration behavior. For a

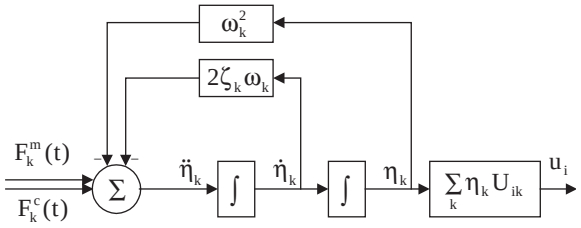

Fig. 2. Open-loop control of a hemispherical shell/actuator system.

free-edge boundary hemispherical shell with the bending approximation, the free-vibration mode shape functions $U_{ik}(\phi,\psi)$ are [1,8,16]

$$U_{\phi k} = -A\left(\tan\frac{\phi}{2}\right)^{k}\sin k\psi, \tag{12}$$

$$U_{\psi k} = -B\sin\phi\left(\tan\frac{\phi}{2}\right)^{k}\cos k\psi, \tag{13}$$

$$U_{3k} = CR(k+\cos\phi)\left(\tan\frac{\phi}{2}\right)^{k}\cos k\psi, \tag{14}$$

where $U_{\phi k}$ is the meridional mode shape function; $U_{\psi k}$ is the circumferential mode shape function; U_{3k} is the radial (transverse) mode shape function; k is the circumferential wave number; ϕ is the meridional angle measured from the pole; ψ is the circumferential angle; and A, B, and C are the modal amplitudes. Natural frequencies of a shallow shell and a thin hemispherical shell with free boundary condition have been studied and experimentally verified [6,7]. To evaluate the control actions, the mechanical excitation is neglected and hence the modal control force $\hat{F}_k(t)$ is defined by actuator induced forces,

$$\hat{F}_k(t) = \frac{1}{\rho h N_k}\int_{\psi}\int_{\phi}\left\{\sum\nolimits_i L_i^c(\phi_3)U_{ik}\right\}R^2\sin\phi\,\mathrm{d}\phi\,\mathrm{d}\psi, \quad i=\phi,\psi,3, \tag{15}$$

where $N_k = \int_{\psi}\int_{\phi}\{\sum_i U_{ik}^2\}R^2\sin\phi\,\mathrm{d}\phi\,\mathrm{d}\psi$; $L_i^c(\phi_3)$ denotes a control operator derived from the converse piezoelectric effect with a transverse control signal ϕ_3 [17]. Detailed microscopic membrane and bending control actions induced by actuator patches are analyzed next.

4. Micro-control actions of actuator patches

Micro-control actions of an arbitrary segmented actuator patch defined from ϕ_1 to ϕ_2 in the meridional direction and from ψ_1 to ψ_2 in the circumferential direction, Fig. 1, are evaluated in this section. It is assumed that the actuator is made of a hexagonal piezoelectric material, i.e., $d_{31} = d_{32}$ and both the actuator and the shell are of uniform thickness. Rewriting the modal control force $\hat{F}_k(t)$ in its meridional, circumferential, and transverse components respectively yields

$$\hat{F}_k(t) = \frac{1}{\rho h N_k}\int_{\psi}\int_{\phi}\{L_{\phi}^c(\phi_3)U_{\phi k} + L_{\psi}^c(\phi_3)U_{\psi k} + L_3^c(\phi_3)U_{3k}\}R^2\sin\phi\,\mathrm{d}\phi\,\mathrm{d}\psi, \tag{16}$$

or

$$\hat{F}_k(t) = \frac{Y_p d_{3i}\phi^a(t)}{\rho}[(\hat{T}_k)_{Total}] = \frac{Y_p d_{3i}\phi^a(t)}{\rho}[(\hat{T}_{k\_merd}) + (\hat{T}_{k\_cir}) + (\hat{T}_{k\_trans})], \quad i=1,2. \tag{17}$$

where $(\hat{T}_k)_{Total}$ denotes the overall actuation action determined by actuator location and modal characteristics, but excluding material constants and modal amplitudes (assumed unity); $(\hat{T}_{k\_merd})$, $(\hat{T}_{k\_cir})$ and $(\hat{T}_{k\_trans})$ respectively denote the actuation magnitudes in the meridional, circumferential and transverse directions defined next. Note that design parameters hN_k are

included in control action expressions and d_{3i} is the piezoelectric constant which will be specifically defined with respect to these control actions later, although $d_{31} = d_{32}$ in commonly used piezoelectric materials. Since the piezoelectric strain constants $d_{31} = d_{32}$ and the effective distance (i.e., moment arm) $r_1^a = r_2^a = r^a$, both the control membrane forces and the control moments are equal, i.e., $N_{\phi\phi}^c = N_{\psi\psi}^c$ and $M_{\phi\phi}^c = M_{\psi\psi}^c$. Using the control force and moment definitions of the actuator patch bounded by ϕ_1 to ϕ_2 and ψ_1 to ψ_2, substituting the mode shape functions and keeping two design parameters hN_k in control actions, one can rewrite the meridional and the circumferential control forces of spherical actuator patches as

$$\begin{aligned}
&\frac{1}{\rho h N_k}\int_{\psi}\int_{\phi} L_{\phi}^c(\phi_3)U_{\phi k}R^2\sin\phi\,\mathrm{d}\phi\,\mathrm{d}\psi\\
&\quad=\frac{1}{\rho h N_k}\int_{\psi_1}^{\psi_2}\int_{\phi_1}^{\phi_2} A\left(\tan\frac{\phi}{2}\right)^k \sin k\psi\sin\phi\cdot(R+r^a)\cdot Y_a d_{31}\phi^a\\
&\qquad\cdot[\delta(\phi-\phi_1)-\delta(\phi-\phi_2)][u_s(\psi-\psi_1)-u_s(\psi-\psi_2)]\,\mathrm{d}\phi\,\mathrm{d}\psi\\
&\quad=\frac{Y_p d_{31}\phi^a}{\rho h N_k}\frac{A}{k}\cdot(R+r^a)\cdot\left[\left(\tan\frac{\phi_1}{2}\right)^k\cdot\sin\phi_1-\left(\tan\frac{\phi_2}{2}\right)^k\cdot\sin\phi_2\right](\cos k\psi_1-\cos k\psi_2)\\
&\quad=\frac{Y_p d_{31}\phi^a(t)}{\rho}[(\hat{T}_{k_merd})],
\end{aligned}\tag{18}$$

$$\begin{aligned}
&\frac{1}{\rho h N_k}\int_{\psi}\int_{\phi} L_{\psi}^c(\phi_3)U_{\psi k}R^2\sin\phi\,\mathrm{d}\phi\,\mathrm{d}\psi\\
&\quad=\frac{1}{\rho h N_k}\int_{\psi_1}^{\psi_2}\int_{\phi_1}^{\phi_2} B\sin\phi\left(\tan\frac{\phi}{2}\right)^k \cos k\psi\cdot(R+r^a)\cdot Y_p d_{32}\phi^a\\
&\qquad\cdot[u_s(\phi-\phi_1)-u_s(\phi-\phi_2)][\delta(\psi-\psi_1)-\delta(\psi-\psi_2)]\,\mathrm{d}\phi\,\mathrm{d}\psi\\
&\quad=\frac{Y_p d_{32}\phi^a}{\rho h N_k}B\cdot(R+r^a)\cdot(\cos k\psi_1-\cos k\psi_2)\int_{\phi_1}^{\phi_2}\sin\phi\left(\tan\frac{\phi}{2}\right)^k\mathrm{d}\phi\\
&\quad=\frac{Y_p d_{32}\phi^a(t)}{\rho}[(\hat{T}_{k_cir})],
\end{aligned}\tag{19}$$

where $\delta(\cdot)$ is a Dirac delta function: $\delta(\phi-\phi^*)=1$ when $\phi=\phi^*$, and $=0$ when $\phi\neq\phi^*$. And, the transverse modal control force can be rewritten as

$$\begin{aligned}
&\frac{1}{\rho h N_k}\int_{\psi}\int_{\phi} L_3^c(\phi_3)U_{3k}R^2\sin\phi\,\mathrm{d}\phi\,\mathrm{d}\psi\\
&\quad=\frac{1}{\rho h N_k}\int_{\psi}\int_{\phi}\left\{\frac{\partial}{\partial\phi}\left[\frac{\partial(M_{\phi\phi}^c\sin\phi)}{\partial\phi}\right]-\frac{\partial}{\partial\phi}(M_{\psi\psi}^c\cos\phi)\right.\\
&\qquad\left.+\frac{1}{\sin\phi}\frac{\partial}{\partial\psi}\left[\frac{\partial(M_{\psi\psi}^c)}{\partial\psi}\right]-R\sin\phi[N_{\phi\phi}^c+N_{\psi\psi}^c]\right\}\\
&\qquad\cdot\left[-CR(k+\cos\phi)\left(\tan\frac{\phi}{2}\right)^k\cos k\psi\right]\mathrm{d}\phi\,\mathrm{d}\psi.
\end{aligned}\tag{20}$$

Note that

$$\frac{\partial}{\partial\phi}\left[\frac{\partial(M^c_{\phi\phi}\sin\phi)}{\partial\phi}\right] = \frac{\partial}{\partial\phi}\left[M^c_{\phi\phi}\cos\phi + \sin\phi\,\frac{\partial(M^c_{\phi\phi})}{\partial\phi}\right]$$
$$= \frac{\partial}{\partial\phi}[M^c_{\phi\phi}\cos\phi] + \frac{\partial}{\partial\phi}\left[\sin\phi\,\frac{\partial(M^c_{\phi\phi})}{\partial\phi}\right]$$
$$= \frac{\partial}{\partial\phi}[M^c_{\phi\phi}\cos\phi] + \sin\phi\,\frac{\partial}{\partial\phi}\left[\frac{\partial(M^c_{\phi\phi})}{\partial\phi}\right] + \cos\phi\,\frac{\partial(M^c_{\phi\phi})}{\partial\phi}$$

and $N^c_{\phi\phi} = N^c_{\psi\psi}$, $M^c_{\phi\phi} = M^c_{\psi\psi}$. Then, the transverse control force is reduced to

$$\frac{1}{\rho h N_k}\int_\psi\int_\phi L^c_3(\phi_3)U_{3k}R^2\sin\phi\,\mathrm{d}\phi\,\mathrm{d}\psi$$
$$= \frac{1}{\rho h N_k}\int_\psi\int_\phi\left\{\sin\phi\,\frac{\partial}{\partial\phi}\left[\frac{\partial(M^c_{\phi\phi})}{\partial\phi}\right] + \cos\phi\,\frac{\partial(M^c_{\phi\phi})}{\partial\phi}\right.$$
$$\left. + \frac{1}{\sin\phi}\frac{\partial}{\partial\psi}\left[\frac{\partial(M^c_{\psi\psi})}{\partial\psi}\right] - R\sin\phi[N^c_{\phi\phi} + N^c_{\psi\psi}]\right\}\cdot\left[-CR(k+\cos\phi)\left(\tan\frac{\phi}{2}\right)^k\cos k\psi\right]\mathrm{d}\phi\,\mathrm{d}\psi$$
$$= \frac{Y_p d_{31}\phi^a(t)}{\rho}[(\hat{T}_{k\_trans})], \tag{21}$$

where the transverse control action $(\hat{T}_{k\_trans})$ and its contributing meridional and circumferential membrane/bending components, i.e., $(\hat{T}_{k\_trans}) = (\hat{T}_{k\_trans})_{\phi,bend} + (\hat{T}_{k\_trans})_{\psi,bend} + (\hat{T}_{k\_trans})_{\phi,mem} + (\hat{T}_{k\_trans})_{\psi,mem}$, will be explicitly defined next. Unlike the meridional and the circumferential control actions, the transverse action requires integration by parts to reveal detailed micro-control characteristics. We analyze the transverse control action in Eq. (21) term by term, beginning with the first term related to the meridional control moment,

$$\frac{1}{\rho h N_k}\int_\psi\int_\phi \sin\phi\,\frac{\partial}{\partial\phi}\left[\frac{\partial(M^c_{\phi\phi})}{\partial\phi}\right]\cdot[-U_{3k}]\,\mathrm{d}\phi\,\mathrm{d}\psi$$
$$= \frac{1}{\rho h N_k}\int_{\psi_1}^{\psi_2}\int_{\phi_1}^{\phi_2} -CR(k+\cos\phi)\left(\tan\frac{\phi}{2}\right)^k\cos k\psi\cdot\sin\phi\cdot r^a Y_p d_{31}\phi^a$$
$$\cdot\frac{\partial}{\partial\phi}[\delta(\phi-\phi_1) - \delta(\phi-\phi_2)][u_s(\psi-\psi_1) - u_s(\psi-\psi_2)]\,\mathrm{d}\phi\,\mathrm{d}\psi$$
$$= \frac{Y_p d_{31}\phi^a}{\rho h N_k}\left(-\frac{C}{k}R\cdot r^a\right)\cdot(\sin k\psi_2 - \sin k\psi_1)\left\{\left[-(k+\cos\phi_2)\left(\tan\frac{\phi_2}{2}\right)^k\sin\phi_2\right.\right.$$
$$\left. - (k+\cos\phi_1)\left(\tan\frac{\phi_1}{2}\right)^k\sin\phi_1\right] - \left[(k^2+2k\cos\phi_1+\cos 2\phi_1)\left(\tan\frac{\phi_1}{2}\right)^k\right.$$
$$\left.\left. - (k^2+2k\cos\phi_2+\cos 2\phi_2)\left(\tan\frac{\phi_2}{2}\right)^k\right]\right\}. \tag{22a}$$

The second term due to the meridional control moment becomes

$$\begin{aligned}
&\frac{1}{\rho h N_k}\int_{\psi}\int_{\phi}\cos\phi\,\frac{\partial(M^c_{\phi\phi})}{\partial\phi}\cdot[-U_{3k}]\,\mathrm{d}\phi\,\mathrm{d}\psi\\
&\quad=\frac{1}{\rho h N_k}\int_{\psi_1}^{\psi_2}\int_{\phi_1}^{\phi_2}-CR(k+\cos\phi)\left(\tan\frac{\phi}{2}\right)^k\cos k\psi\cdot\cos\phi\cdot r^a Y_p d_{31}\phi^a\\
&\qquad\cdot[\delta(\phi-\phi_1)-\delta(\phi-\phi_2)][u_s(\psi-\psi_1)-u_s(\psi-\psi_2)]\,\mathrm{d}\phi\,\mathrm{d}\psi\\
&\quad=\frac{Y_p d_{31}\phi^a}{\rho h N_k}\left(-\frac{CR}{k}\cdot r^a\right)\cdot(\sin k\psi_2-\sin k\psi_1)\\
&\qquad\cdot\left[(k+\cos\phi_1)\left(\tan\frac{\phi_1}{2}\right)^k\cos\phi_1-(k+\cos\phi_2)\left(\tan\frac{\phi_2}{2}\right)^k\cos\phi_2\right].
\end{aligned}\tag{22b}$$

Combining Eqs. (22a) and (22b) yields the control action from the meridional control moment: $[Y_p d_{31}\phi^a(t)/\rho][(\hat{T}_{k\_trans})_{\phi,bend}]$. Then, the third term of the circumferential control moment in the transverse control action becomes

$$\begin{aligned}
&\frac{1}{\rho h N_k}\int_{\psi}\int_{\phi}\frac{1}{\sin\phi}\frac{\partial}{\partial\psi}\left[\frac{\partial(M^c_{\psi\psi})}{\partial\psi}\right]\cdot[-U_{3k}]\,\mathrm{d}\phi\,\mathrm{d}\psi\\
&\quad=\frac{1}{\rho h N_k}\int_{\psi_1}^{\psi_2}\int_{\phi_1}^{\phi_2}-CR(k+\cos\phi)\left(\tan\frac{\phi}{2}\right)^k\cos k\psi\cdot\frac{1}{\sin\phi}\cdot r^a Y_p d_{32}\phi^a\\
&\qquad\cdot[u_s(\phi-\phi_1)-u_s(\phi-\phi_2)]\frac{\partial}{\partial\psi}[\delta(\psi-\psi_1)-\delta(\psi-\psi_2)]\,\mathrm{d}\phi\,\mathrm{d}\psi\\
&\quad=\frac{Y_p d_{32}\phi^a}{\rho h N_k}(-CR\cdot r^a)\{(-\cos k\psi_2-\cos k\psi_1)+k(\sin k\psi_1-\sin k\psi_2)\}\\
&\qquad\times\int_{\phi_1}^{\phi_2}(k+\cos\phi)\left(\tan\frac{\phi}{2}\right)^k\frac{1}{\sin\phi}\,\mathrm{d}\phi\\
&\quad=\frac{Y_p d_{32}\phi^a(t)}{\rho}[(\hat{T}_{k_trans})_{\psi,bend}].
\end{aligned}\tag{22c}$$

Finally, the fourth term of the transverse action related to the meridional and circumferential membrane control forces becomes

$$\begin{aligned}
&\frac{1}{\rho h N_k}\int_{\psi}\int_{\phi}-R\sin\phi[N^c_{\phi\phi}+N^c_{\psi\psi}]\cdot[-U_{3k}]\,\mathrm{d}\phi\,\mathrm{d}\psi\\
&\quad=\frac{1}{\rho h N_k}\int_{\psi_1}^{\psi_2}\int_{\phi_1}^{\phi_2}2CR^2(k+\cos\phi)\left(\tan\frac{\phi}{2}\right)^k\cos k\psi\cdot\sin\phi\cdot Y_p d_{31}\phi^a\\
&\qquad\cdot[u_s(\phi-\phi_1)-u_s(\phi-\phi_2)][u_s(\psi-\psi_1)-u_s(\psi-\psi_2)]\,\mathrm{d}\phi\,\mathrm{d}\psi
\end{aligned}$$

$$= \frac{Y_p d_{31}\phi^a}{\rho h N_k}\left(2\frac{C}{k}R^2\right)\cdot(\sin k\psi_2 - \sin k\psi_1)\int_{\phi_1}^{\phi_2}(k+\cos\phi)\left(\tan\frac{\phi}{2}\right)^k \sin\phi\,\mathrm{d}\phi$$

$$= \frac{Y_p d_{31}\phi^a(t)}{\rho}[(\hat{T}_{k\_trans})_{\phi,mem} + (\hat{T}_{k\_trans})_{\psi,mem}]. \tag{22d}$$

Note that the meridional and the circumferential membrane control forces (i.e., $N^c_{\phi\phi}$ and $N^c_{\psi\psi}$) appear equal, due to the two piezoelectric constants $d_{31} = d_{32}$ in hexagonal piezoelectric materials and each contributes one half the total membrane control action in the above equation. Accordingly, all three control forces and their detailed micro-control actions in the total control force $\hat{F}_k(t) = (1/\rho h N_k)\int_\psi\int_\phi\{L^c_\phi(\phi_3)U_{\phi k} + L^c_\psi(\phi_3)U_{\psi k} + L^c_3(\phi_3)U_{3k}\cdot R^2\sin\phi\,\mathrm{d}\phi\,\mathrm{d}\psi$ are defined and its simplified microscopic contributing meridional/circumferential bending and membrane control components: $\hat{F}_k(t) = [Y_p d_{3i}\phi^a(t)/\rho][(\hat{T}_k)_{Total}] = [Y_p d_{3i}\phi^a(t)/\rho][(\hat{T}_{k\_merd}) + (\hat{T}_{k\_cir}) + (\hat{T}_{k\_trans})]$ are respectively derived in Eqs. (18), (19), and (22a–d), and their detailed microscopic control actions can be rewritten as

$$(\hat{T}_{k\_merd}) = (\hat{T}_{k\_mer})_{\phi,bend} + (\hat{T}_{k\_mer})_{\psi,bend} + (\hat{T}_{k\_mer})_{\phi,mem} + (\hat{T}_{k\_mer})_{\psi,mem}, \tag{23}$$

$$(\hat{T}_{k\_cir}) = (\hat{T}_{k\_cir})_{\phi,bend} + (\hat{T}_{k\_cir})_{\psi,bend} + (\hat{T}_{k\_cir})_{\phi,mem} + (\hat{T}_{k\_cir})_{\psi,mem}, \tag{24}$$

$$(\hat{T}_{k\_trans}) = (\hat{T}_{k\_trans})_{\phi,bend} + (\hat{T}_{k\_trans})_{\psi,bend} + (\hat{T}_{k\_trans})_{\phi,mem} + (\hat{T}_{k\_trans})_{\psi,mem}, \tag{25}$$

where $(\hat{T}_k)_{\phi,bend}$ and $(\hat{T}_k)_{\psi,bend}$ denote the bending control moment actions resulting from $M^c_{\phi\phi}$ and $M^c_{\psi\psi}$; $(\hat{T}_k)_{\phi,mem}$ and $(\hat{T}_k)_{\psi,mem}$ denote the membrane control force actions resulting from $N^c_{\phi\phi}$ and $N^c_{\psi\psi}$ respectively. Note that the transverse meridional bending control action $(\hat{T}_{k\_trans})_{\phi,bend}$ is the summation of Eqs. (22a) and (22b) and the transverse circumferential bending control action $(\hat{T}_{k\_trans})_{\psi,bend}$ is equal to Eq. (22c). The total membrane control action, Eq. (22d), consists of a transverse meridional membrane control action $(\hat{T}_{k\_trans})_{\phi,mem}$ and a transverse circumferential membrane control action $(\hat{T}_{k\_trans})_{\psi,mem}$. Since the effective moment arm $r^a_1 = r^a_2 = r^a$ and the piezoelectric constants $d_{31} = d_{32}$, magnitudes of these two membrane actions are equal, i.e., $(\hat{T}_{k\_trans})_{\phi,mem} = (\hat{T}_{k\_trans})_{\psi,mem}$. These detailed microscopic modal control actions and components corresponding to various design and geometric parameters are analyzed in case studies presented next.

5. Parametric study of active vibration control

A systematic study of actuator characteristics, micro-control actions, and control effectiveness of segmented actuator patches on free-edge hemispheric shells is presented in this section. Parametric analyses of design parameters, such as actuator position, shell thickness, shell curvature, etc., are conducted to evaluate actuator characteristics and microscopic control actions. Standard dimensions of the hemispherical shell are as follows: shell curvature radius $R = 1$ m, shell thickness $h = 0.01$ m, and piezoelectric actuator thickness $h^a = 40$ μm. Effects of dimensional changes are compared with those derived from these standard dimensions. Other actuator material constants and control signal, e.g., $Y_p d_{31}\phi^a(t)/\rho$, are assumed constant, such that control forces can be calculated when actuator materials and signals are specified. Note that

although the current piezoelectric materials may not be strong enough to achieve effective control, these parametric analyses still reveal the actuator's spatial control actions and desirable locations for various natural mode controls.

Control characteristics of natural modes ($k = 2, 3, 4$) are evaluated in case studies. Since the in-plane meridional and circumferential vibrations are usually small as compared with the transverse vibration, this study primarily focuses on control effects and micro-control actions that are essential to the transverse vibration, i.e., $(\hat{T}_{k\_trans})$. The transverse modal control force $(\hat{T}_k)_{Total}$ and its micro-contributing components, i.e., $(\hat{T}_k)_{\phi,bend}$, $(\hat{T}_k)_{\psi,bend}$, $(\hat{T}_k)_{\phi,mem}$ and $(\hat{T}_k)_{\psi,mem}$, related to actuator positions, shell thickness, shell curvature, etc. are evaluated next.

5.1. Actuator patch positions

The segmented actuator patches are laminated on the shell at 0–10, 10–20, 20–30, …, 80–90 meridian degrees and the patch is circumferentially divided at every $(2n-1)\pi/(2k)$ radians where n is the number of divisions, $n = 1, 2, 3, \ldots, 2k$, and k is the circumferential wave number. Note that the circumferential division, i.e., $(2n-1)\pi/(2k)$, assures that the patches are divided based on nodal lines without any phase shift, such that the maximal control effect can be achieved. Fig. 3 illustrates the actuator patch segmentation designed for the 4th hemispheric shell mode.

The overall modal control force of patch actuators (i.e., including the surface integration over the patch) is calculated for the $k = 2, 3, 4$ natural modes. With the segmented actuator patches designed as discussed previously, i.e., $(2n-1)\pi/(2k)$, the in-plane control actions $(\hat{T}_{k\_mer})$ and $(\hat{T}_{k\_cir})$ are zero, due to the spatial effect that $\cos k\psi_1$ and $\cos k\psi_2$ become zero when specific circumferential angles are considered in Eqs. (18) and (19). Thus, only the transverse control action $(\hat{T}_{k\_trans})$ contributes to the overall control action $(\hat{T}_k)$, which includes (1) micro-control actions induced by control moments, i.e., $(\hat{T}_{k\_trans})_{\phi,bend}$ and $(\hat{T}_{k\_trans})_{\psi,bend}$, and (2) those induced by membrane control forces, i.e., $(\hat{T}_{k\_trans})_{\phi,mem}$ and $(\hat{T}_{k\_trans})_{\psi,mem}$. The total transverse control actions $(\hat{T}_{k\_trans})$ for the $k = 2, 3, 4$ modes at various patch locations (from 0–90°) are calculated and plotted in Fig. 4. Detailed microscopic meridional and circumferential control actions including the membrane control components and the bending moment control components for

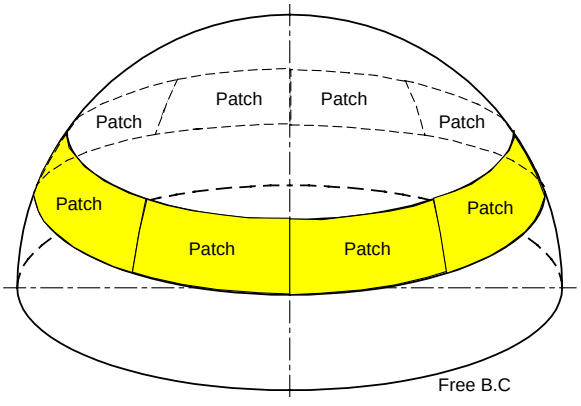

Fig. 3. Piezoelectric actuator patch positions for the $k = 4$ mode.

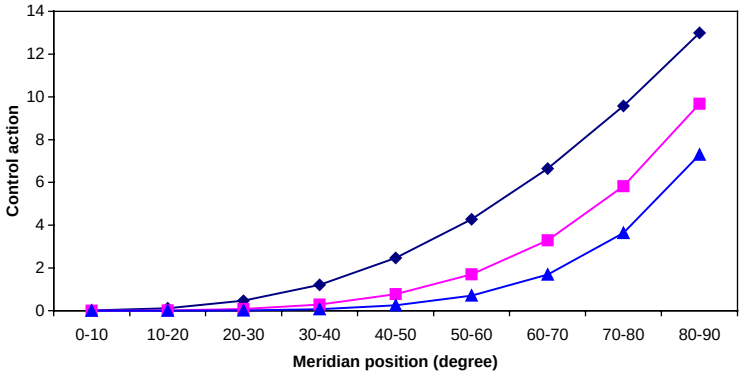

Fig. 4. Total modal control action ($\hat{T}_{k\_trans}$) at various actuator locations ($k = 2, 3, 4$). ♦: $k = 2$ mode; ▩: $k = 3$ mode; ▲: $k = 4$ mode.

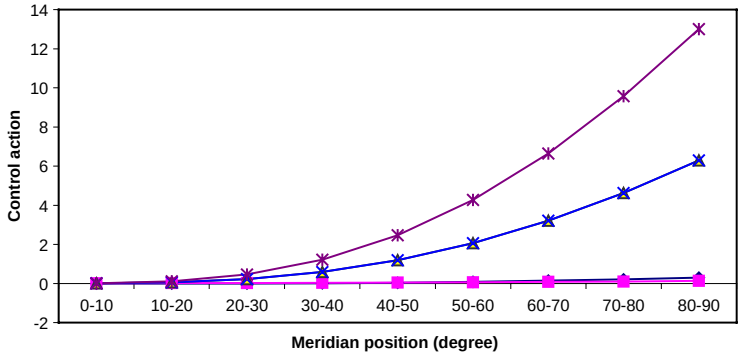

Fig. 5. Micro-modal control actions at various actuator locations ($k = 2$). ♦: $(\hat{T}_{k\_trans})_{\phi,bend}$; ▩: $(\hat{T}_{k\_trans})_{\psi,bend}$; △: $(\hat{T}_{k\_trans})_{\phi,mem}$; ×: $(\hat{T}_{k\_trans})_{\psi,mem}$; ∗: $(\hat{T}_k)$.

the $k = 2, 3, 4$ modes are respectively calculated and summarized in Figs. 5–7, and so is N_k plotted in Fig. 8.

Fig. 4 illustrates that the control action increases when the actuator patch moves from the pole to the free edge and it decreases at higher natural modes. Observing Figs. 5–7 suggests that (1) the total control action decreases when the circumferential wave number (or the mode) increases and (2) the membrane components, $(\hat{T}_k)_{\phi,mem}$ and $(\hat{T}_k)_{\psi,mem}$, dominate the overall control action. Fig. 8 shows that N_k increases when the mode increases, which results in a reduced control action at higher modes, since $h \times N_k$ is on the denominator of the control force definition.

5.2. Shell thickness

The bending behavior becomes relatively significant in a thicker shell. Variation of shell thickness is to evaluate the thickness effect to actuation characteristics. The hemispherical shell thickness is assumed to be changing from 1 to 6 cm, while the standard shell radius R remains at

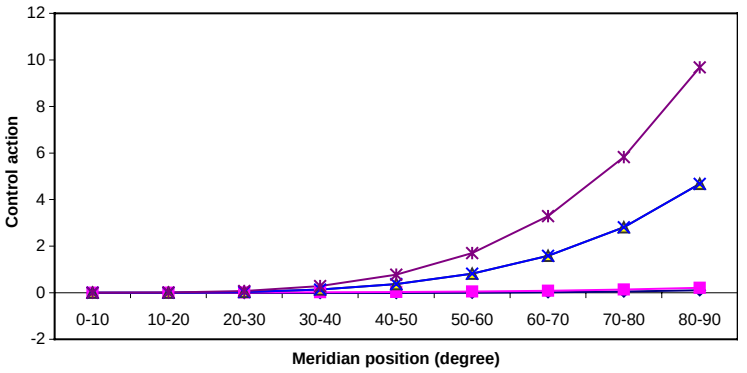

Fig. 6. Modal control actions at various actuator locations ($k = 3$). ♦: $(\hat{T}_{k\_trans})_{\phi,bend}$; ▩: $(\hat{T}_{k\_trans})_{\psi,bend}$; △: $(\hat{T}_{k\_trans})_{\phi,mem}$; ×: $(\hat{T}_{k\_trans})_{\psi,mem}$; ∗: $(\hat{T}_k)$.

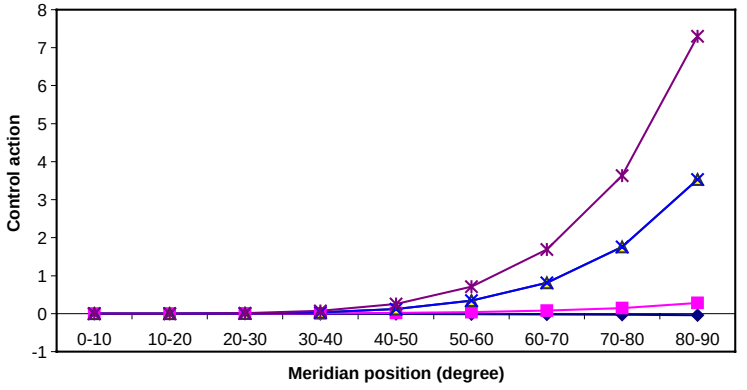

Fig. 7. Modal control actions at various actuator locations ($k = 4$). ♦: $(\hat{T}_{k\_trans})_{\phi,bend}$; ▩: $(\hat{T}_{k\_trans})_{\psi,bend}$; △: $(\hat{T}_{k\_trans})_{\phi,mem}$; ×: $(\hat{T}_{k\_trans})_{\psi,mem}$; ∗: $(\hat{T}_k)$.

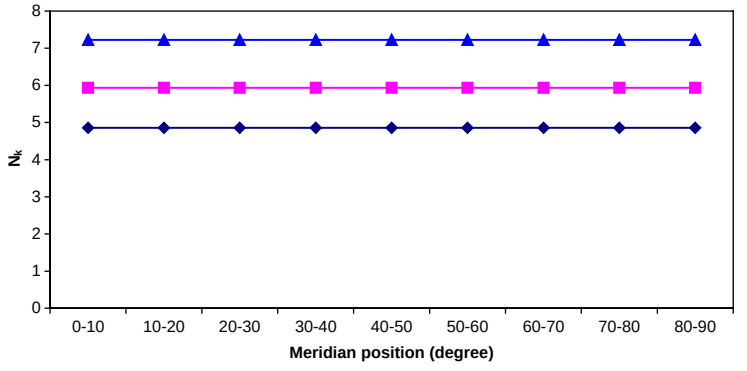

Fig. 8. N_k at various actuator locations ($k = 2, 3, 4$). ♦: $k = 2$ mode; ▩: $k = 3$ mode; ▲: $k = 4$ mode.

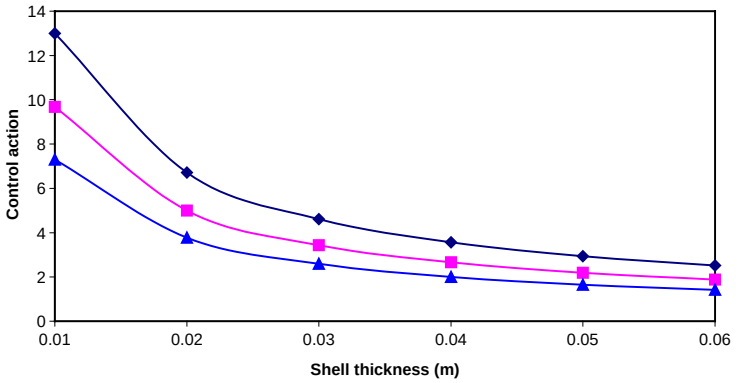

Fig. 9. Total modal patch control action ($\hat{T}_{k\_trans}$) at various shell thickness (position 80–90°, $R = 1$ m, $k = 2, 3, 4$). ◆: $k = 2$ mode; ▩: $k = 3$ mode; ▲: $k = 4$ mode.

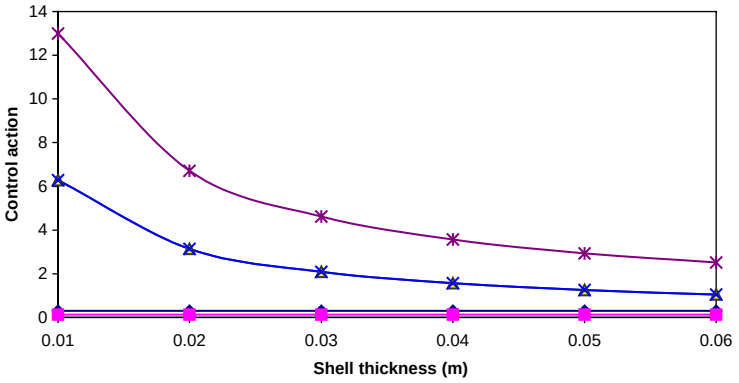

Fig. 10. Modal control actions at various shell thickness (position 80–90°, $R = 1$ m, $k = 2$). ◆: $(\hat{T}_{k\_trans})_{\phi,bend}$; ▩: $(\hat{T}_{k\_trans})_{\psi,bend}$; △: $(\hat{T}_{k\_trans})_{\phi,mem}$; ×: $(\hat{T}_{k\_trans})_{\psi,mem}$; ✱: $(\hat{T}_k)$.

1 m or diameter of 2 m. The piezoelectric actuator thickness h^a is 40 μm, located at 80–90° meridian, and the actuators are circumferentially segmented at every $(2n-1)\pi/(2k)$ radians where $n = 1, 2, 3, \ldots, 2k$. The patch control forces of the $k = 2$–4 modes are analyzed and plotted in Fig. 9. It shows that the control action decreases when the shell thickens, due to increased flexible rigidity, and it also decreases at higher natural modes. Detailed $k = 2$–4 modal micro-control actions of various shell thickness are also calculated and plotted in Figs. 10–12.

These data suggest, again, that the micro-membrane control actions dominate the overall control action and the control action decreases when the shell thickens or at higher natural modes. The membrane control force is usually independent of shell thickness, i.e., Eqs. (2) and (3). However, the micro-control actions $(\hat{T}_k)_{\phi,mem}$ and $(\hat{T}_k)_{\psi,mem}$ are defined in Eq. (22d), resulting in a reduction of $(\hat{T}_k)_{\phi,mem}$ and $(\hat{T}_k)_{\psi,mem}$ when the shell thickness h increases. On the other hand, the bending control actions $(\hat{T}_k)_{\phi,bend}$ and $(\hat{T}_k)_{\psi,bend}$ usually influenced by the transverse location

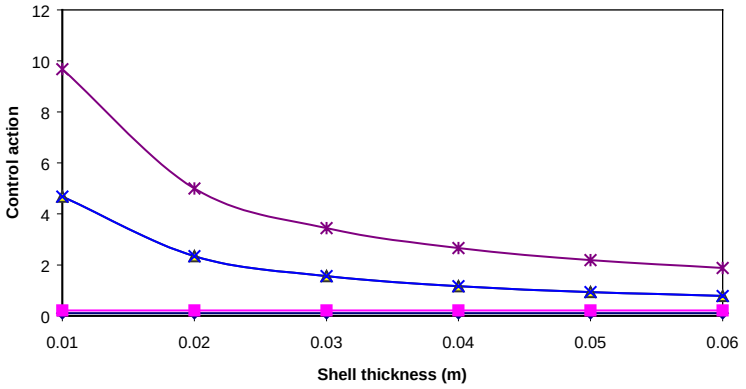

Fig. 11. Modal control actions at various shell thickness (position 80–90°, $R = 1$ m, $k = 3$). ◆: $(\hat{T}_{k\_trans})_{\phi,bend}$; ▩: $(\hat{T}_{k\_trans})_{\psi,bend}$; △: $(\hat{T}_{k\_trans})_{\phi,mem}$; ×: $(\hat{T}_{k\_trans})_{\psi,mem}$; ∗: $(\hat{T}_k)$.

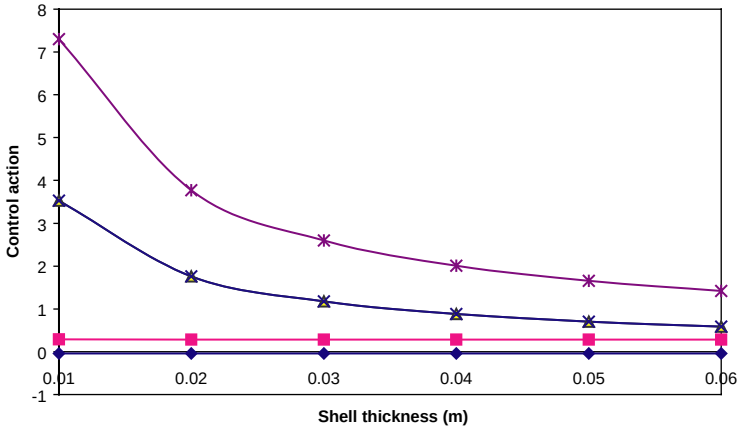

Fig. 12. Modal control actions at various shell thickness (position 80–90°, $R = 1$ m, $k = 4$). ◆: $(\hat{T}_{k\_trans})_{\phi,bend}$; ▩: $(\hat{T}_{k\_trans})_{\psi,bend}$; △: $(\hat{T}_{k\_trans})_{\phi,mem}$; ×: $(\hat{T}_{k\_trans})_{\psi,mem}$; ∗: $(\hat{T}_k)$.

$r^a = (h/2 + h^a/2)$, i.e., Eqs. (4) and (5), show little variation, since the actions are defined in Eqs. (22a, b) and $h^a/(h \times N_k)$ is very small.

5.3. Radius of curvature

Next, the hemispherical shell radius changes from 1 to 2 m, with a standard shell thickness $h = 0.01$ m. The piezoelectric actuator thickness h^a remains at 40 μm, located at 80–90° meridian, and the actuators are circumferentially segmented at every $(2n-1)\pi/(2k)$ radians. The patch actuator induced control actions of modes $k = 2, 3, 4$ are presented in Fig. 13, in which the modal control action decreases as the radius of curvature increases or at higher natural modes. Detailed micro-control actions resulting from the meridional/circumferential membrane/bending components of modes $k = 2, 3, 4$ are respectively calculated and plotted in Figs. 14–16. Again,

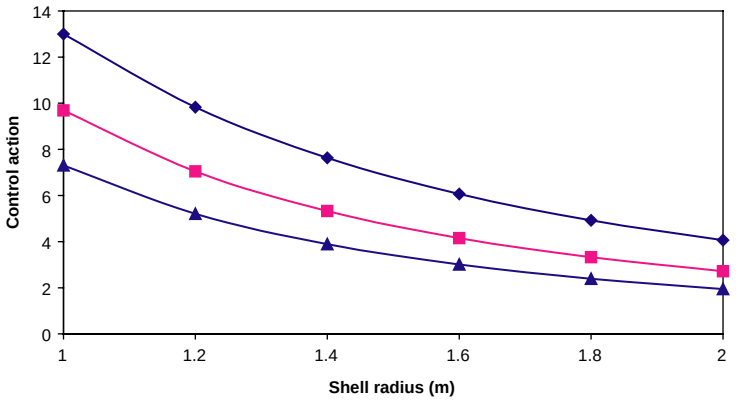

Fig. 13. Total modal patch control actions ($\hat{T}_{k\_trans}$) at various shell radius (position 80–90°, $h = 0.01$ m, $k = 2, 3, 4$). ♦: $k = 2$ mode; ▩: $k = 3$ mode; ▲: $k = 4$ mode.

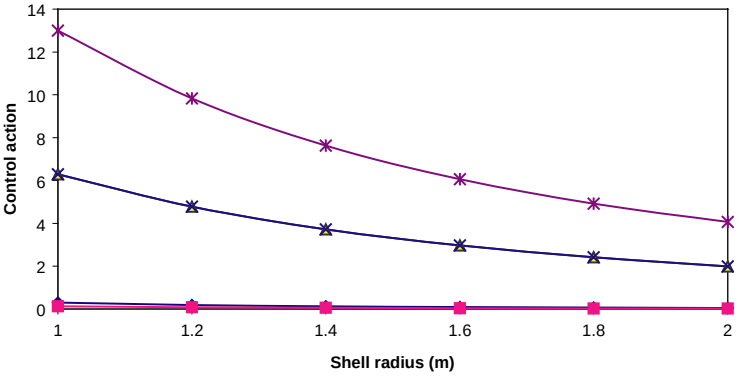

Fig. 14. Modal control actions at various shell radius (position 80–90°, $h = 0.01$ m, $k = 2$). ♦: $(\hat{T}_{k\_trans})_{\phi,bend}$; ▩: $(\hat{T}_{k\_trans})_{\psi,bend}$; △: $(\hat{T}_{k\_trans})_{\phi,mem}$; ×: $(\hat{T}_{k\_trans})_{\psi,mem}$; ∗: $(\hat{T}_k)$.

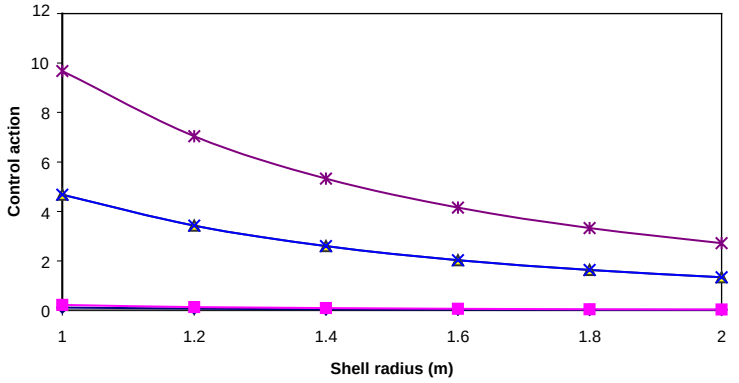

Fig. 15. Modal control actions at various shell radius (position 80–90°, $h = 0.01$ m, $k = 3$). ♦: $(\hat{T}_{k\_trans})_{\phi,bend}$; ▩: $(\hat{T}_{k\_trans})_{\psi,bend}$; △: $(\hat{T}_{k\_trans})_{\phi,mem}$; ×: $(\hat{T}_{k\_trans})_{\psi,mem}$; ∗: $(\hat{T}_k)$.

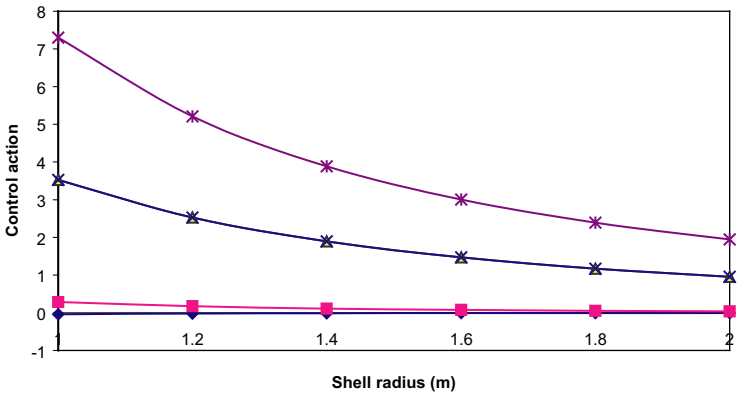

Fig. 16. Modal control actions at various shell radius (position 80–90°, $h = 0.01$ m, $k = 4$). ♦: $(\hat{T}_{k\_trans})_{\phi,bend}$; ▩: $(\hat{T}_{k\_trans})_{\psi,bend}$; △: $(\hat{T}_{k\_trans})_{\phi,mem}$; ×: $(\hat{T}_{k\_trans})_{\psi,mem}$; ∗: $(\hat{T}_k)$.

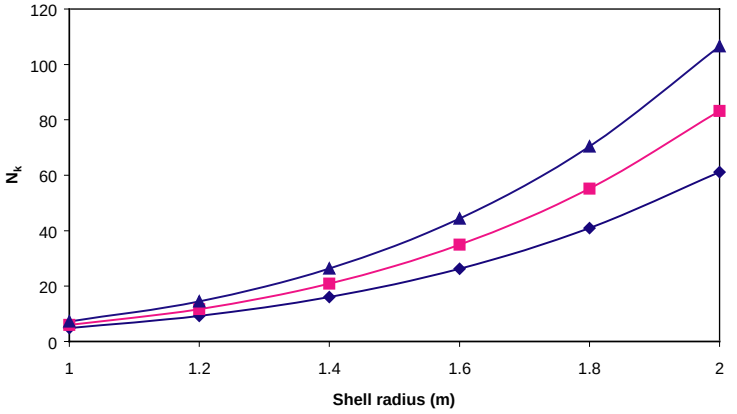

Fig. 17. N_k at various shell radius ($k = 2, 3, 4$). ♦: $k = 2$ mode; ▩: $k = 3$ mode; ▲: $k = 4$ mode.

these data indicate that the primary contributing components are the two micro-membrane control actions which decrease due to increased radius of curvature.

Fig. 17 shows that N_k significantly increases as the radius increases, resulting in reduction of control actions as the radius increases. And similar to the first two cases, N_k increases at higher modes and it causes reduction of control actions at higher natural modes.

5.4. Control effectiveness

With the segmentation technique described previously, i.e., segmented at every $(2n-1)\pi/(2k)$, the effective actuator area actually increases as the actuator patch moving from the pole down to the boundary rim and it decreases as the natural mode k increases. Fig. 18 illustrates three types ($k = 2, 3, 4$) of actuator layouts and their actuator size variations. Fig. 19 shows the effective actuator area of three types of layouts increases as the shell radius increases.

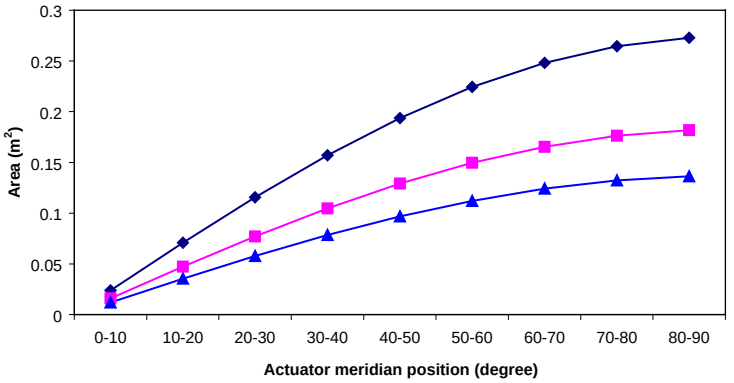

Fig. 18. Effective actuator sizes at various patch locations ($R = 1$ m). ♦: type $k = 2$; ▩: type $k = 3$; ▲: type $k = 4$.

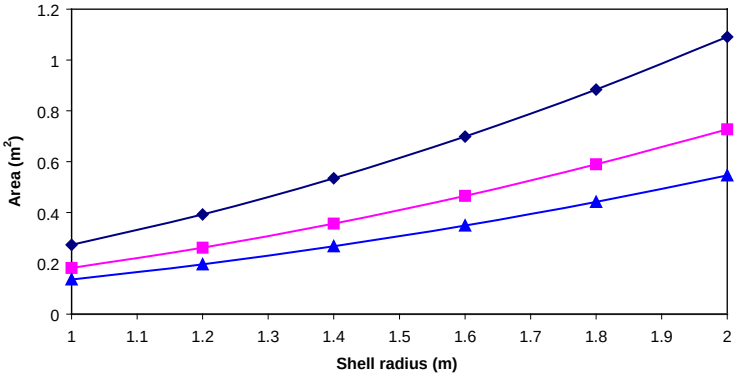

Fig. 19. Effective actuator sizes versus shell radiuses (position 80–90°). ♦: type $k = 2$; ▩: type $k = 3$; ▲: type $k = 4$.

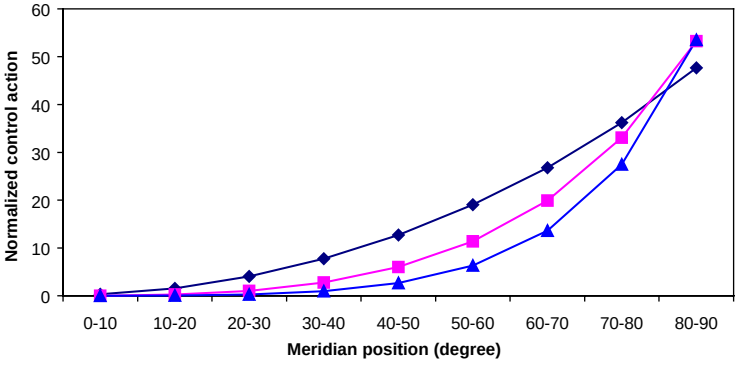

Fig. 20. Normalized control actions at various locations ($R = 1$ m, $h = 0.01$ m). ♦: $k = 2$ mode; ▩: $k = 3$ mode; ▲: $k = 4$ mode.

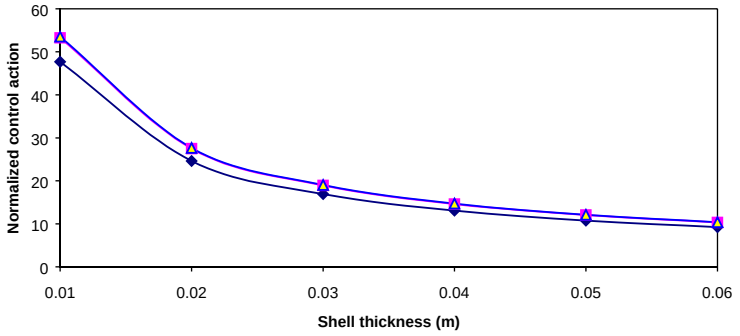

Fig. 21. Normalized control actions at various shell thickness (position 80–90°, $R = 1$ m). ◆: $k = 2$ mode; ▩: $k = 3$ mode; ▲: $k = 4$ mode.

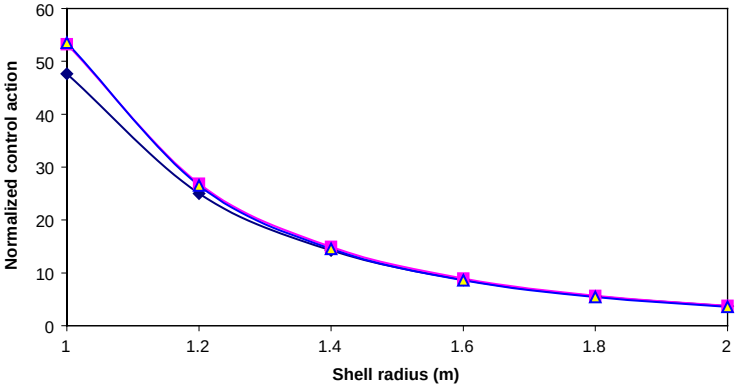

Fig. 22. Normalized control actions at various shell radius (position 80–90°, $h = 0.01$ m). ◆: $k = 2$ mode; ▩: $k = 3$ mode; ▲: $k = 4$ mode.

Since the actuator sizes are not constant, consequently the control actions need to be normalized such that the true control authority per actuator area can be inferred. These effective (normalized) control actions of three actuator layouts are presented in Figs. 20–22. These data suggest that (1) the effective control effect reaches maximal at the free edge, positioned at 80–90° meridian, Fig. 20, (2) the effective control action decreases as the shell thickness increases, Fig. 21, and (3) the effective (normalized) control action decreases when the shell radius increases, Fig. 22.

6. Conclusions

Actuation and control of hemispherical shells using segmented distributed piezoelectric actuators are investigated in this study. Mathematical models for spherical/hemispherical shells laminated with distributed actuator layers were defined first, followed by formulations of distributed control forces and their contributing microscopic meridional/circumferential membrane and bending control actions based on a simplified bending approximation theory.

Detailed modal control forces, directional micro-control actions, and normalized control effects of free-edge hemispheric shells with various geometric parameters (or design parameters) were evaluated. With a delicate modal-dependent segmentation mechanism, i.e., $(2n-1)\pi/(2k)$, effects of the in-plane meridional and circumferential control forces are eliminated from the overall control actions and that of the transverse control action is retained. The total control action $(\hat{T}_k)_{Total}$ depends on actuator locations and modal characteristics, excluding actuator material properties and control signals. The modal control force $\hat{F}_k(t)$ can be inferred from the control action by multiplying actuator parameters, i.e., $Y_p d_{31}\phi^a(t)/\rho$, when specific piezoelectric actuator and control signals are selected. Qualitative parametric analyses of hemispheric shells with segmented patch actuators suggest that (1) the micro-meridional/circumferential membrane control actions dominate the overall modal control force; (2) the modal patch control force increases as the actuator patch moves toward the free edge; (3) the actuation magnitude decreases at higher natural modes; (4) the modal control force decreases as the shell thickens, due to increased shell rigidity; (5) the modal control force decreases as the radius of curvature increases and the shell radius significantly influences the nominal value of N_k; (6) the effective actuator size enlarges as the patch location moving from the pole to the free boundary rim for a specified k; and (7) the effective (or normalized) actuator induced control action reaches maximal at the free edge and it decreases as the shell thickness or the shell radius increases.

These generic guidelines can be applied to design of segmented actuator patches, their spatial layouts, and control effectiveness of precision hemispheric shells.

Acknowledgements

This research is supported, in part, by a grant (F49620-98-1-0467) from the Air Force Office of Scientific Research (Project Manager: Brian Sanders). This support is gratefully acknowledged.

References

[1] J.W. Strutt, B. Rayleigh, *Theory of Sound*, Vol. 1, 2nd Edition, Dover Publications, New York, 1945, pp. 418–432.
[2] A. Kalnins, Effect of bending on vibrations of spherical shells, *The Journal of The Acoustical Society of America* 36 (1) (1964) 74–81.
[3] W.E. Baker, Axisymmetric modes of vibration of thin spherical shells, *The Journal of The Acoustical Society of America* 33 (12) (1961) 1749–1758.
[4] A.K. Eikrem, A.G. Doige, Natural frequencies of a hemispherical shell, *Experimental Mechanics* 12 (1972) 575–579.
[5] Z.E. Mazurkiewicz, R.T. Nagorski, *Shells of Revolution*, PWN-Polish Scientific Publishers, Warsaw, 1991, pp. 7–9, 333–341.
[6] M.W. Johnson, E. Reissner, On inextensional deformations of shallow elastic shells, *Journal of Mathematics and Physics* 34 (1956) 335–346.
[7] C. Hwang, Some experiments on the vibration of a hemispherical shell, *Journal of Applied Mechanics* 33 (1966) 817–824.
[8] H.S. Tzou, P. Smithmaitrie, J.H. Ding, Micro-sensor electromechanics and distributed signal analysis of piezo(electric)-elastic spherical shells, *Mechanical Systems and Signal Processing* 16 (2–3) (2002) 185–199.
[9] V. Jayachandran, J.Q. Sun, Modeling shallow-spherical-shell piezoceramic actuators as acoustic boundary control elements, *Smart Materials and Structures* 7 (1) (1998) 72–84.

[10] V. Birman, S. Griffin, G. Knowles, Axisymmetric dynamics of composite spherical shells with active piezoelectric/composite stiffeners, *Acta Mechanica* 141 (1) (2000) 71–83.
[11] S.K. Ghaedi, A.K. Misra, Active control of shallow spherical shells using piezoceramic sheets, *Proceedings of SPIE—The International Society for Optical Engineering*, v 3668 n II, Mar 1999, pp. 890–912.
[12] H.S. Tzou, D.W. Wang, W.K. Chai, Dynamics and distributed control of conical shells laminated with full and diagonal actuators, *Journal of Sound and Vibration* 256 (1) (2002) 65–79.
[13] H.S. Tzou, J.H. Ding, I. Hagiwara, Micro-control actions of segmented actuator patches laminated on deep paraboloidal shells, *JSME International Journal Series C* 45 (1) (2002) 8–15.
[14] H.S. Tzou, Thin-layer distributed piezoelectric neurons and muscles: electromechanics and applications, in: H.S. Tzou, T. Fukuda (Eds.), *Precision Sensors, Actuators, and Systems*, Kluwer Academic Publishers, Dordrecht/Boston/London, 1992, pp. 175–218.
[15] R.V. Howard, W.K. Chai, H.S. Tzou, Modal voltages of linear and nonlinear structures using distributed artificial neurons (a theoretical and experimental study), *Mechanical Systems and Signal Processing* 15 (3) (2001) 629–640.
[16] R.D. Blevins, *Formulas for Natural Frequency And Mode Shape*, Reprint Ed., Krieger Publisher Company, Florida, 1987, pp. 330–336.
[17] H.S. Tzou, *Piezoelectric Shells (Distributed Sensing and Control of Continua)*, Kluwer Academic Publishers, Boston/Dordrecht, 1993.